PHYSICAL REVIEW B **89**, 220407(R) (2014)

Commensurate-incommensurate magnetic phase transition in the Fe-doped bilayer ruthenate $Ca_3Ru_2O_7$

X. Ke,[1,*] J. Peng,[2,3] W. Tian,[4] Tao Hong,[4] M. Zhu,[1] and Z. Q. Mao[2]

[1]*Department of Physics and Astronomy, Michigan State University, East Lansing, Michigan 48824, USA*

[2]*Department of Physics and Engineering Physics, Tulane University, New Orleans, Louisiana 70118, USA*

[3]*Laboratory of Solid State Microstructures and Department of Physics, Nanjing University, Nanjing 210093, China*

[4]*Quantum Condensed Matter Division, Oak Ridge National Laboratory, Oak Ridge, Tennessee 37831, USA*

(Received 2 April 2014; published 23 June 2014)

Neutron diffraction studies have revealed an uncommon commensurate-incommensurate magnetic phase transition with decreasing temperature in the (∼5%) Fe-doped bilayer ruthenate $Ca_3(Ru,Fe)_2O_7$. An incommensurate phase formed of a cycloidal spiral spin structure coexists with a commensurate one below the phase transition at 42 K and persists down to the lowest temperature, accompanied by higher-order magnetic satellite peaks which indicate the formation of a magnetic soliton lattice. We ascribe these findings to the competing magnetic interactions in this system. This study demonstrates an effective approach to tune novel magnetic and electronic properties of ruthenates via 3*d* magnetic transition-metal substitution.

DOI: 10.1103/PhysRevB.89.220407 PACS number(s): 75.25.−j, 75.40.Cx, 75.47.Lx

Layered ruthenate oxides with extended 4*d* electron orbitals are known to have comparable values of electron-electron Coulomb interaction U and bandwidth W [1], and thus exhibit a rich variety of competing ground states with nearly equivalent energies. This makes this system extremely susceptible to external stimuli, such as chemical doping, magnetic fields, pressure, etc. For instance, because of the competition due to ferromagnetic and antiferromagnetic fluctuations, while Sr_2RuO_4 is a spin-triplet superconductor [2], $(Sr_{1-x}Ca_x)_2RuO_4$ shows novel phases with different Ca concentration [3] and eventually leads to a Mott insulator state with G-type antiferromagnetic ordering for Ca_2RuO_4 due to the structural distortion induced by Ca [4,5]; on the other hand, $Sr_2(Ru_{1-x}Ti_x)O_4$ with nonmagnetic isovalent Ti^{4+} dopants becomes an insulator with incommensurate spin density wave ordering [6,7].

The bilayer ruthenate $Ca_3Ru_2O_7$ is another interesting material attracting intense attention recently. This material possesses a $Bb_{21}m$ orthorhombic crystal structure with the lattice parameters $a = 5.378$ Å, $b = 5.522$ Å, and $c = 19.587$ Å [8]. It is a metallic paramagnet at high temperature and undergoes an antiferromagnetic transition at $T_N \approx 56$ K [9] with ferromagnetic bilayers coupled antiferromagnetically [8,10,11] and spins aligned along the a axis (AFM-a), as depicted in Figs. 1(a) and 1(b). This is followed by a first-order metal-insulator transition at $T_{MIT} \approx 48$ K where the same magnetic structure holds, but spins switch to the b axis (AFM-b) [11]. Recently it was found [12,13] that doping Ti onto Ru sites leads to a Mott insulator ground state with G-type antiferromagnetic structure in $Ca_3(Ru_{1-x}Ti_x)_2O_7$ where Ti^{4+} ions with $3d^0$ electron orbital strongly scatter carriers. This suggests that $Ca_3Ru_2O_7$ is on the verge of Mott insulator with a strong interplay between ferromagnetic and antiferromagnetic correlations.

In this Rapid Communication, we report an uncommon commensurate (C)-incommensurate (IC) magnetic phase transition upon cooling in the bilayer ruthenate $Ca_3Ru_2O_7$ induced by a modest amount of Fe doped onto Ru sites, a feature drastically different from both the pristine and Ti-doped compounds. The C phase shares a similar spin structure to the pure compound, i.e., AFM-a, above the metal-insulator transition temperature T_{MIT}. The IC phase characterized by a cycloidal spiral spin structure occurs below T_{MIT} and coexists with another C phase (i.e., AFM-b). Furthermore, the IC phase is accompanied by the formation of magnetic solitons that persists at low temperatures. We ascribe these findings to the delicate balance of competing magnetic interactions that are tuned by Fe dopants.

Single-phase $Ca_3(Ru_{0.95}Fe_{0.05})_2O_7$ single crystals were grown using a floating-zone technique. The Fe doping concentration of the samples was verified using the energy dispersive spectroscopy method. The magnetic, electronic, and thermodynamic properties of these crystals were measured using a Quantum Design PPMS and SQUID magnetometer, respectively. Neutron diffraction experiments were performed using the HB1A neutron triple-axis spectrometer located at High Flux Isotope Reactor (HFIR), Oak Ridge National Laboratory. The neutron incident energy E_i was fixed as 14.62 meV and data were taken with collimations of 48′-48′-sample-40′-68′. A high-quality single crystal sample with a mass of ≈ 70 mg was cooled down using a closed-cycle He fridge. Note that the sample for neutron study has a twin domain with the ratio of the twins being ≈0.12:1 and the twins are orthogonal to each other in the ab plane. The sample was measured in the $(H\ 0\ L)$ and $(H\ H\ L)$ scattering planes of the larger domain, with H, K, and L being the reciprocal lattice indices. Both H (K) and L need to be even or the sum of H and L needs to be even for nuclear Bragg reflections.

Figures 2(a) and 2(b) show the temperature dependence of magnetization and heat capacity of $Ca_3(Ru_{0.95}Fe_{0.05})_2O_7$, respectively. For comparison, the corresponding data of pure $Ca_3Ru_2O_7$ were plotted in the insets. Similar to the parent compound, two marked magnetic phase transitions are observed in $Ca_3(Ru_{0.95}Fe_{0.05})_2O_7$: one at $T_N \approx 80$ K corresponding to the paramagnet-antiferromagnet transition [14], and the other one at about 42 K (denoted as T_{MIT}). The span of these two transition temperatures is much wider than that observed in

*ke@pa.msu.edu

 ©2014 American Physical Society

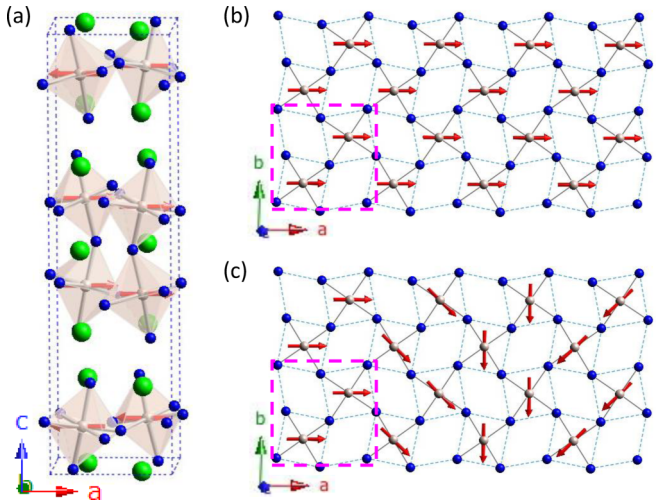

FIG. 1. (Color online) (a) Schematic spin structure (AFM-a) of $Ca_3Ru_2O_7$ and $Ca_3(Ru_{0.95}Fe_{0.05})_2O_7$ at $T_{MIT} < T < T_N$. (b) In-plane view of the AFM-a type magnetic structure showing the ferromagnetic spin alignment. (c) In-plane view of the spiral magnetic structure of $Ca_3(Ru_{0.95}Fe_{0.05})_2O_7$ at $T < T_{MIT}$ with the propagation vector along the [1 0 0] axis. The pink dashed frames in (b) and (c) represent the repeating unit cell.

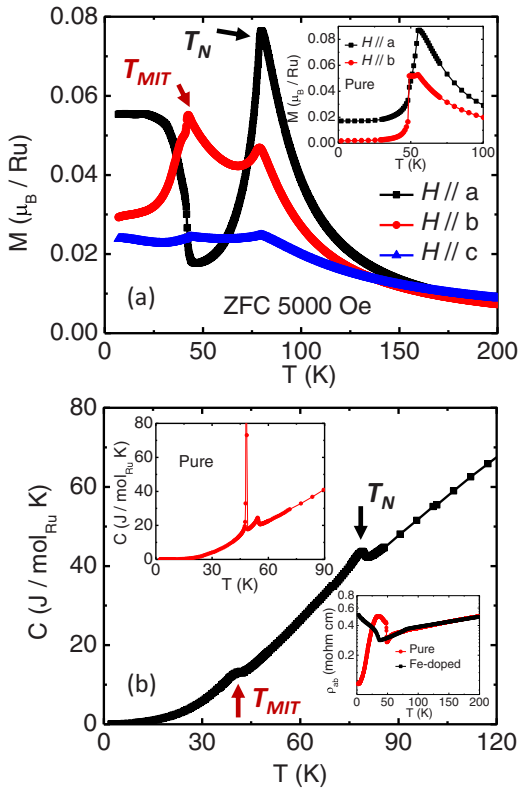

FIG. 2. (Color online) (a) Temperature dependence of magnetization of $Ca_3(Ru_{0.95}Fe_{0.05})_2O_7$ measured with a 5000 Oe field applied along different crystalline axes. The data were taken after the sample was cooled down at zero field (ZFC). Inset shows the magnetization data of pure $Ca_3Ru_2O_7$ for comparison. (b) Temperature dependence of specific heat of $Ca_3(Ru_{0.95}Fe_{0.05})_2O_7$. The left top inset is the specific heat data of $Ca_3Ru_2O_7$ for comparison, and the right bottom inset shows the in-plane resistivity as a function of temperature for both compounds. Arrows point to the onset of two magnetic phase transitions.

pure $Ca_3Ru_2O_7$. It is worth noting that $Ca_3(Ru_{0.95}Fe_{0.05})_2O_7$ shows several features that are in remarkable contrast to $Ca_3Ru_2O_7$: (i) As shown in Fig. 2(a), the magnetization of $Ca_3(Ru_{0.95}Fe_{0.05})_2O_7$ with field applied along the a axis sharply increases below T_{MIT}. (ii) The phase transition at T_{MIT} belongs to the second-order type as suggested by the small λ-shape peak in the specific heat data shown in Fig. 2(b), as compared to the large sharp peak observed at T_{MIT} in $Ca_3Ru_2O_7$. (iii) $Ca_3(Ru_{0.95}Fe_{0.05})_2O_7$ behaves as an insulator below T_{MIT}, while $Ca_3Ru_2O_7$ shows metallic behavior below 30 K. These characteristics suggest a distinct magnetic and electronic ground state of $Ca_3(Ru_{0.95}Fe_{0.05})_2O_7$ from both pure $Ca_3Ru_2O_7$ and the Ti-doped $Ca_3(Ru_{1-x}Ti_x)_2O_7$.

To determine the magnetic structure of $Ca_3(Ru_{0.95}Fe_{0.05})_2O_7$, comprehensive neutron diffraction experiments were carried out. It is known that the propagation vector of the magnetic structure of $Ca_3Ru_2O_7$ is (0 0 1) [8,11] and its magnetic neutron scattering intensity increases monotonically with decreasing temperature with a sudden jump at T_{MIT} [11,12]. Figure 3(a) shows the temperature dependence of several magnetic reflections measured in both (H 0 L) and (H H L) planes. The neutron intensity of the (0 0 5) reflection as illustrated by black symbols increases below $T_N \sim 80$ K, indicating the onset of the antiferromagnetic transition. Intriguingly, this is followed by a drastic drop at $T_{MIT} \approx 42$ K and then a slight increase with a "bump" between 15 and 32 K. Such a feature is dramatically different from either the monotonic increase of the (0 0 5) intensity observed in $Ca_3Ru_2O_7$ [8,12] or the negligible intensity in the 3% Ti-doped $Ca_3Ru_2O_7$ below T_{MIT} [12], which implies distinct ground-state magnetic structures among these three compounds. The main panel of Fig. 3(b) shows a contour map of (H 0 5)-T near the (0 0 5) reflection. There is a sole magnetic reflection with an intensity maximum at (0 0 5) for $T_{MIT} < T < T_N$, while two extra magnetic diffractions occur below T_{MIT} and persist down to $T = 4$ K in addition to the (0 0 5) Bragg peak that has a smaller intensity. These two satellite peaks appear at (δ 0 5) with $\delta \approx \pm 0.017$, as seen from the black symbols (a line cut at $T = 10$ K) shown in the bottom inset, characteristic of an IC magnetic structure [14]. This suggests a C-IC magnetic phase transition at T_{MIT} with a coexistence of both IC and C magnetic structures at low temperatures, a feature in sharp contrast to the IC-C spontaneous phase transition upon cooling that is more commonly observed [15–22]. Surprisingly, we find the incommensurability δ is almost temperature independent with $|\Delta\delta| < 0.0015$ even at the temperature close to the phase transition (within 1 K limit). This is distinct from the gradual increase of incommensurability reported in other systems such as CuB_2O_4 [23] and $NdFe_3(^{11}BO_3)_4$ [24] which could be well fitted by the sine-Gordon equation. Detailed temperature dependence of the neutron intensity of the IC diffraction (0.017 0 5) is illustrated by the red curve shown in Fig. 3(a) with its onset being coincident with the drop in intensity of the C diffraction (0 0 5) at T_{MIT}. Note that there is a slight change in the lattice constants [shown in the top inset of

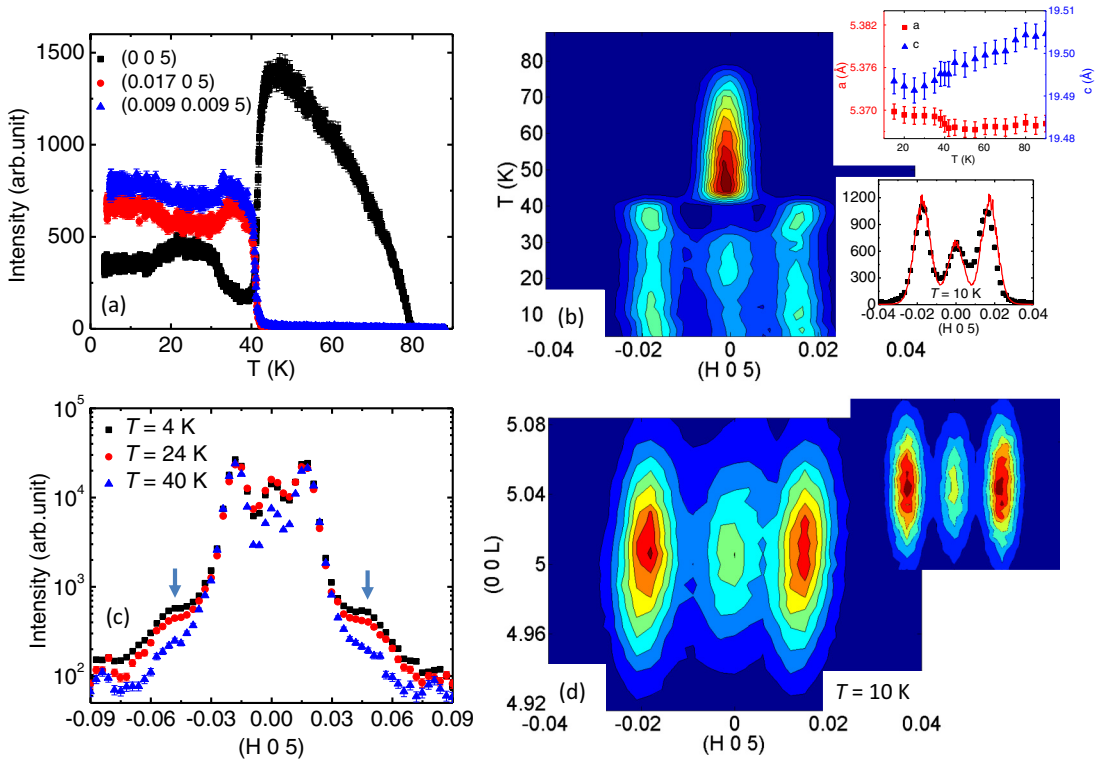

FIG. 3. (Color online) Temperature dependence of magnetic diffraction intensity of (0 0 5) and (0.017 0 5) measured in the (H 0 L) plane and (0.009 0.009 5) measured in the (H H L) plane of $Ca_3(Ru_{0.95}Fe_{0.05})_2O_7$. (b) ($H$ 0 5)-T contour map of the neutron intensity. The top inset shows the temperature dependence of a and c lattice constants and the bottom figure is a $\boldsymbol{Q}$ scan over the (0 0 5) magnetic reflection at T = 10 K. The red solid curve is the calculated result taking into account the instrumental resolution. (c) Extended $\boldsymbol{Q}$ scans over the (0 0 5) magnetic reflection measured at different temperatures showing both first- and third-order satellites. The position of the third-order one is indicated by the arrows. (d) (H 0 5)-(0 0 L) contour map of the neutron intensity around the (0 0 5) magnetic Bragg measured at T = 10 K. Inset shows the corresponding contour map of the calculated intensity as described in the text.

Fig. 3(b)] at T_{MIT}, indicative of the magnetoelastic coupling, which is much smaller than that observed in the pristine [8] and Ti-doped compounds [12].

An (H 0 5)-(0 0 L) contour map measured at T = 10 K is shown in Fig. 3(d). Diffraction measurements were also conducted in the (H H L) plane. The main panel of Fig. 4(a) shows the (H H 5)-T contour map where the IC diffractions at (δ' δ' 5) are observed below T_{MIT}, with $\delta' \approx 0.0085$, about half value of δ; δ' again is nearly independent of temperature. And the temperature dependence of neutron scattering intensity of the IC diffraction at (0.009 0.009 5) is illustrated by the blue curve in Fig. 3(a). The IC feature is also clearly indicated by the (H H 5)-(0 0 L) contour map in the inset of Fig. 4(a) and the line cuts cross L = 5 at various temperatures shown in Figs. 4(b)–4(d).

A complete set of magnetic reflections was collected at T = 50 K (above T_{MIT}) and T = 10 K (below T_{MIT}), and we found that the commensurate magnetic structure of $Ca_3(Ru_{0.95}Fe_{0.05})_2O_7$ above T_{MIT} [14] is the same as that of pure $Ca_3Ru_2O_7$, which is denoted as AFM-a type as represented by Figs. 1(a) and 1(b). On the other hand, the commensurate phase that coexists with the incommensurate one below T_{MIT} has a magnetic structure similar to AFM-a, but with the magnetization easy axis aligned along the b axis (i.e., the AFM-b phase). A similar transition from AFM-a to AFM-b across T_{MIT} also occurs in undoped $Ca_3Ru_2O_7$; however, $Ca_3Ru_2O_7$ does not show any IC component below T_{MIT} [11].

The observed incommensurate diffraction peaks in the vicinity of the commensurate (0 0 5) Bragg peak suggest that the modulated magnetic structure below T_{MIT} has a predominant antiferromagnetic component. To account for these observations, we considered the most reasonable magnetic model with a cycloid spin spiral structure shown in Fig. 1(c) where the relative Ru spin orientations within a unit cell (indicated by pink dashed frame) are the same as those in the commensurate AFM-b phase but the direction of moments is sinusoidal modulated from cell to cell with the wave vector $q_m \approx$ (0.017 0 0) along the a axis and spins rotating in the ab plane. To validate this model, we calculated the neutron scattering intensity using the RESLIB program package [25] which convolutes the instrumental resolution. Effects of the twin domain and the coexisting C phase were taken into account. The magnetic structure factor of the IC phase is expressed as $S(\boldsymbol{Q}) \sim G(\boldsymbol{Q} - \tau + q_m) + G(\boldsymbol{Q} - \tau - q_m)$ using a Gaussian approximation $G(x)$. And it is $S(\boldsymbol{Q}) \sim G(\boldsymbol{Q} - \tau)$ for the commensurate phase. Here $\boldsymbol{Q}$ is the wave vector transfer, $\boldsymbol{\tau}$ is (0 0 5) corresponding to the fundamental antiferromagnetic Bragg diffraction, and $\boldsymbol{q_m}$ is the propagation wave vector, which is (0.017 0 0). The calculated neutron intensity distribution illustrated by the (H 0 5)-(0 0 L) contour map, which is shown in the inset of Fig. 3(d), and the calculated

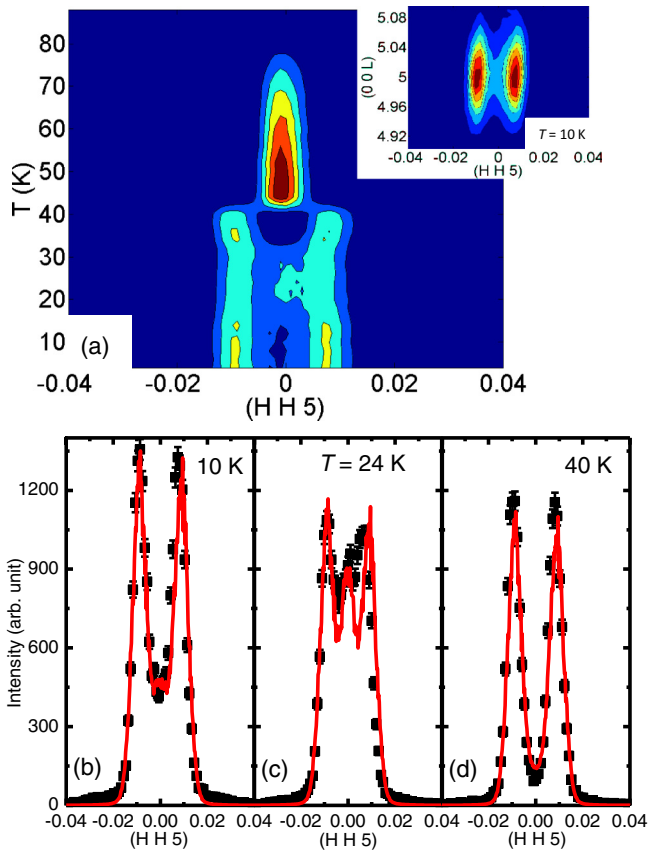

FIG. 4. (Color online) (a) (H H 5)-T contour map of the neutron intensity measured in the (H H L) plane. The inset depicts the (H H 5)-(0 0 L) contour map of the neutron intensity at $T = 10$ K. (b)–(d) show $\boldsymbol{Q}$ scans over the (0 0 5) magnetic reflection at $T = 10$,24, and 40 K, respectively. Red solid curves are calculated intensities as described in the text with ratio of the commensurate phase to the incommensurate phase of the sample being about 0.17, 0.40, and 0.05 for these three temperatures, respectively.

line cut cross $L = 5$, which is represented by the red curve in the bottom inset of Fig. 3(b), are in very good agreement with the experimental data. This suggests the validity of the proposed cycloid spiral spin structure shown in Fig. 3(c). The magnetic modulation length is about 32 nm, and the spin rotates by an angle of ≈6.2° about the c axis relative to spins in the adjacent unit cell.

The coexistence of the C and IC phases below T_{MIT} implies phase competition in the chemically homogeneous $Ca_3(Ru_{0.95}Fe_{0.05})_2O_7$ that exhibits a sole T_N at 80 K. The ratio of the C phase to the IC one varies with temperature, as indicated by the nonmonotonic temperature dependence of neutron scattering intensity of the commensurate (0 0 5) and incommensurate (0.017 0 5) and (0.009 0.009 5) magnetic reflections shown in Fig. 3(a) and contour maps in Figs. 3(b) and 4(a), respectively. Quantitatively, fits to the (H H 5) data measured at $T = 10$,24, and 40 K presented in Figs. 4(b)–4(d) give a ratio of the C phase to the IC one of about 17%, 40%, and 5%, respectively.

In addition to the satellite peaks appearing at (±0.017 0 5), we also observed third-order reflections of the modulated IC magnetic structure positioning at (±0.051 0 5) as depicted in Fig. 3(c). Third-order harmonics also occurred in a constant $\boldsymbol{Q}$ scan of (H H 5). These suggest the formation of a magnetic soliton lattice originating from the deviation of the spiral spin structure from the uniform spatial propagation [26]. The spontaneous formation of a magnetic soliton lattice was previously observed in $TbFeO_3$ [22], CuB_2O_4 [23], and $NdFe_3(^{11}BO_3)_4$ [24], and magnetic-field-induced solitons have also been reported in $Ba_2CuGe_2O_7$ [27]. However, it is intriguing to note that the magnetic soliton lattice in $Ca_3(Ru_{0.95}Fe_{0.05})_2O_7$ persists down to the lowest temperature $T = 4$ K with stronger neutron scattering intensity for the third-order satellite peaks at lower temperature than those at higher temperatures. This is in sharp contrast to the previously reported cases [22–24] where the higher-order magnetic satellites only exist or display largest neutron intensity in the vicinity of C-IC phase transition.

In contrast to $TbFeO_3$ with a centrosymmetric crystal lattice in which the occurrence of IC magnetic structure and magnetic solitons originates from the stabilization of domain walls [22], our findings in $Ca_3(Ru_{0.95}Fe_{0.05})_2O_7$ at low temperatures can be ascribed to two possible mechanisms [28,29]. One scenario is associated with the Dzyaloshinskii-Moriya (DM) interaction described by Lifshitz invariants in combination with spin anisotropy [28]. Indeed, the DM interaction is allowed in $Ca_3(Ru_{0.95}Fe_{0.05})_2O_7$ due to its noncentrosymmetric crystal structure [8] with an off-center displacement of Ru atoms along the b axis, i.e., the [0 1 0] direction. In this case, the spin-spin interaction between neighboring spins along the a axis as shown in Fig. 1(c), although it is a second-nearest-neighbor interaction, can give rise to the magnetic incommensurability [14]. The DM interaction has been attributed to the occurrence of IC magnetic structures in improper multiferroic materials such as $CaMn_7O_{12}$ in which a structural modulation also exists and intertwines with the IC magnetic structure [30]. In addition, the known magnetic anisotropy of ruthenates [11] is expected to distort the uniform spiral propagation. Such a mechanism has been applied to interpret the formation of magnetic solitons in CuB_2O_4 [23] and $NdFe_3(^{11}BO_3)_4$ [24]. Therefore, the DM interaction combined with the materials strong magnetic anisotropy seems to be a plausible mechanism to account for the experimental observations in this study. However, we argue that this is not the main driving force based on the fact that pure $Ca_3Ru_2O_7$ does not exhibit an IC magnetic phase despite its noncentrosymmetric lattice structure.

The other scenario for the appearance of IC magnetic phase is due to competing magnetic interactions [17,28]. While undoped $Ca_3Ru_2O_7$ exhibits the AFM-b type magnetic structure with ferromagnetic bilayers antiferromagnetically coupled along the c axis below T_{MIT} [11], a small percentage (∼3%) of Ti substituted onto Ru sites induces G-type antiferromagnetic spin structure with nearest-neighboring spins antiferromagnetically coupled to each other [12]. This suggests a delicate competition between ferromagnetic and antiferromagnetic interactions in $Ca_3Ru_2O_7$. Therefore, magnetic modulation is likely to occur in this system due to the balance of these interactions and is susceptible to external stimuli. Indeed, this is what we observed here in $Ca_3(Ru_{0.95}Fe_{0.05})_2O_7$. The formation of a magnetic soliton lattice is thus presumably associated with these competing magnetic interactions together with the persistent coexistence of commensurate AFM-**b** and IC phases at low temperatures.

In addition, different from the first scenario in which the temperature-dependent magnetic anisotropy or DM interaction leads to the temperature dependence of incommensurability in CuB_2O_4 [23] and $NdFe_3(^{11}BO_3)_4$, respectively [24], the temperature-independent δ in $Ca_3(Ru_{0.95}Fe_{0.05})_2O_7$ may be attributable to the competing magnetic interactions. Further theoretical modeling or *ab initio* calculation is warranted for verification.

In summary, we have observed an uncommon C-IC magnetic phase transition upon decreasing temperature in the Fe-doped $Ca_3Ru_2O_7$ and attribute the persistent coexistence of C and IC magnetic phases and the formation of a magnetic soliton lattice at low temperatures to competing magnetic interactions. Our study demonstrates an effective approach to tune the novel physical properties of the 4*d* electronically correlated system by substituting 3*d* dopants.

X.K. acknowledges the support from the start-up funds at Michigan State University. Research at Oak Ridge National Laboratory's High Flux Isotope Reactor was sponsored by the Scientific User Facilities Division, Office of Basic Energy Sciences, US Department of Energy. Work at Tulane is supported by the NSF under Grant No. DMR-1205469. J.P. also acknowledges the support from the National Science Foundation of China (NNSFC) under Grant No. 11304149.

[1] G. Cao, C. S. Alexander, S. McCall, J. E. Crow, and R. P. Guertin, Mater. Sci. Eng. B **63**, 76 (1999).
[2] Y. Maeno, H. Hashimoto, K. Yoshida, S. Nishizaki, T. Fujita, J. Bednorz, and F. Lichtenberg, Nature (London) **372**, 532 (1994).
[3] S. Nakatsuji and Y. Maeno, Phys. Rev. Lett. **84**, 2666 (2000).
[4] G. Cao, S. McCall, M. Shepard, J. E. Crow, and R. P. Guertin, Phys. Rev. B **56**, R2916 (1997).
[5] M. Braden, G. André, S. Nakatsuji, and Y. Maeno, Phys. Rev. B **58**, 847 (1998).
[6] M. Minakata and Y. Maeno, Phys. Rev. B **63**, 180504(R) (2001).
[7] M. Braden, O. Friedt, Y. Sidis, P. Bourges, M. Minakata, and Y. Maeno, Phys. Rev. Lett. **88**, 197002 (2002).
[8] Y. Yoshida, S. I. Ikeda, H. Matsuhata, N. Shirakawa, C. H. Lee, and S. Katano, Phys. Rev. B **72**, 054412 (2005).
[9] G. Cao, S. C. McCall, J. E. Crow, and R. P. Guertin, Phys. Rev. Lett. **78**, 1751 (1997).
[10] D. J. Singh and S. Auluck, Phys. Rev. Lett. **96**, 097203 (2006).
[11] W. Bao, Z. Q. Mao, Z. Qu, and J. W. Lynn, Phys. Rev. Lett. **100**, 247203 (2008).
[12] X. Ke, J. Peng, D. J. Singh, T. Hong, W. Tian, C. R. Dela Cruz, and Z. Q. Mao, Phys. Rev. B **84**, 201102(R) (2011).
[13] J. Peng, X. Ke, G. Wang, D. Fobes, T. Hong, W. Tian, X. Wu, and Z. Q. Mao, Phys. Rev. B **87**, 085125 (2013).
[14] See Supplemental Material at http://link.aps.org/supplemental/10.1103/PhysRevB.89.220407 for further discussion of the magnetic ordering and magnetic structure of this material.
[15] H. Lin, L. Rebelsky, M. F. Collins, J. D. Garrett, and W. J. L. Buyers, Phys. Rev. B **43**, 13232 (1991).
[16] T. Chattopadhyay, P. J. Brown, P. Thalmeier, and H. G. v. Schnering, Phys. Rev. Lett. **57**, 372 (1986).
[17] T. Chattopadhyay, Science **264**, 226 (1993), and references therein.
[18] D. Vaknin, J. L. Zarestky, J.-P. Rivera, and H. Schmid, Phys. Rev. Lett. **92**, 207201 (2004).
[19] T. Kimura, Annu. Rev. Mater. Res. **37**, 387 (2007), and references therein.
[20] K. Taniguchi, N. Abe, T. Takenobu, Y. Iwasa, and T. Arima, Phys. Rev. Lett. **97**, 097203 (2006).
[21] Y. Xiao, Y. Su, H. F. Li, C. M. N. Kumar, R. Mittal, J. Persson, A. Senyshyn, K. Gross, and Th. Brueckel, Phys. Rev. B **82**, 094437 (2010).
[22] S. Artyukhin, M. Mostovoy, N. P. Jensen, D. Le, K. Prokes, V. G. de Paula, H. N. Bordallo, A. Maljuk, S. Landsgesell, H. Ryll, B. Klemke, S. Paeckel, K. Kiefer, K. Lefmann, L. T. Kuhn, and D. N. Argyriou, Nat. Mater. **11**, 694 (2012).
[23] B. Roessli, J. Schefer, G. A. Petrakovskii, B. Ouladdiaf, M. Boehm, S. Staub, A. Vorotinov, and L. Bezmaternikh, Phys. Rev. Lett. **86**, 1885 (2001).
[24] M. Janoschek, P. Fischer, J. Schefere, B. Roessli, V. Pomjakushin, M. Meven, V. Petricek, G. Petrakovskii, and L. Bezmaternikh, Phys. Rev. B **81**, 094429 (2010).
[25] See http://www.neutron.phys.ethz.ch/personal/reslib/index.html
[26] A. M. Kosevich, B. A. Ivanov, and A. S. Kovalev, Phys. Rep. **194**, 117 (1990).
[27] A. Zheludev, S. Maslov, G. Shirane, Y. Sasago, N. Koide, and K. Uchinokura, Phys. Rev. Lett. **78**, 4857 (1997).
[28] Y. A. Izyumov, Physica B **174**, 9 (1991).
[29] Y. A. Izyumov and V. M. Laptev, Sov. Phys. JETP **58**, 1267 (1983).
[30] N. J. Perks, R. D. Johnson, C. Martin, L. C. Chapon, and P. G. Radaelli, Nat. Commun. **3**, 1277 (2012).